Investigation of rotating spoke instabilities in a wall-less Hall thruster. Part II: Simulation.

IEPC-2017-403

Presented at the 35th International Electric Propulsion Conference
Georgia Institute of Technology • Atlanta, Georgia • USA
October 8 – 12, 2017

K. Matyash[1], R. Schneider[2],
Greifswald University, Greifswald, D-17487, Germany

S. Mazouffre[3], S. Tsikata[4] and L. Grimaud[5]
ICARE, Centre National de la Recherche Scientifique, 45071 Orléans, France

Abstract: The 3 dimensional Particle-in-Cell code STOIC was applied to simulate the low-frequency rotating plasma instabilities in the ISCT200 thruster operating in the wall-less configuration. In the simulations a spoke rotating with the velocity of about 3-5 km/s was observed. For the most of the simulated regimes the $m = 1$ mode was present with a few occurrences of $m = 2$ mode. The spokes were rotating both in the ExB and in counter-ExB directions. The spoke rotation is associated with azimuthal depletion of the neutral gas, which indicates the ionization nature of the spoke instability. In the simulations the electron cross-field transport in the spoke bulk was caused by diffusion in high-frequency, short-scale electric fields. The electron conductivity at the spoke front was due to ExB drift toward the anode in the low-frequency macroscopic spoke electric field.

Nomenclature

B	=	magnetic field
E	=	electric field
c_s	=	ion acoustic speed
$\dot{m}$	=	mass flow rate
n_e	=	electron density
T_e	=	electron temperature
I	=	electric current
U_a	=	anode voltage
Δx	=	cell size
X, Y, Z	=	coordinates
Δt	=	time step
ϕ	=	electric potential
φ	=	oscillation phase

[1] Head of HPC group, Greifswald University, knm@ipp.mpg.de
[2] Professor, Greifswald University, Head of Computer Center, schneider@uni-greifswald.de
[3] Head of electric propulsion team, ICARE, CNRS, stephane.mazouffre@cnrs-orleans.fr
[4] Research Physicist, ICARE, CNRS, sedina.tsikata@cnrs-orleans.fr
[5] PhD student, ICARE, lou.grimaud@cnrs-orleans.fr

I. Introduction

The low-frequency rotating plasma instability, often called "rotating spoke" is a phenomenon frequently observed in various cross-field discharges like Hall thrusters, magnetrons and plasma columns[1]. In the Hall thrusters, despite decades of investigation, the origin, dynamics and nature of the spoke are still poorly understood. The earliest spoke study, carried out by Janes and Lowder[2], identified an azimuthal structure moving at tens of kilometers per second, whose presence was later attributed to the ionization type instability[3]. Our recent Particle-in-Cell (PIC) simulations of the CHT thruster[4] have also pointed out at the ionization nature of the spoke instability. However, this hypothesis still needs to be validated both theoretically and experimentally.

In a Hall thruster, the spoke instability is of prime importance because it has been shown to be present under any operating conditions, with the mode number varying according to the thruster size and operating conditions[5]. The spoke is of interest principally because it can conduct current, thereby participating in anomalous electron transport[5-7]. Measurements performed in CHT thruster have demonstrated that a large fraction of electron current towards the anode flows through the spoke[6,7]. Probe measurements of the time-evolution of the azimuthal electric field also reveal that the electric field generated by the spoke is responsible for axial electron current.

In this contribution we applied the 3D PIC code STOIC[4,8] to investigate the properties of low-frequency rotating plasma instabilities in the discharge of the low power ISCT200 Hall thruster[9,10] operating in wall-less configuration[11,12]. The main objective of this work was to characterize the dynamics of rotating plasma structures in the *E*x*B* discharge of ISCT200 and to provide the insight into the physics of the rotating spoke instability by means of self-consistent PIC simulations.

Notice the experimental investigation of rotating spokes in the discharge of our 200W Hall thruster will be presented in a companion paper, see IEPC paper 2017-248[13].

II. ISCT200-WL Hall thruster

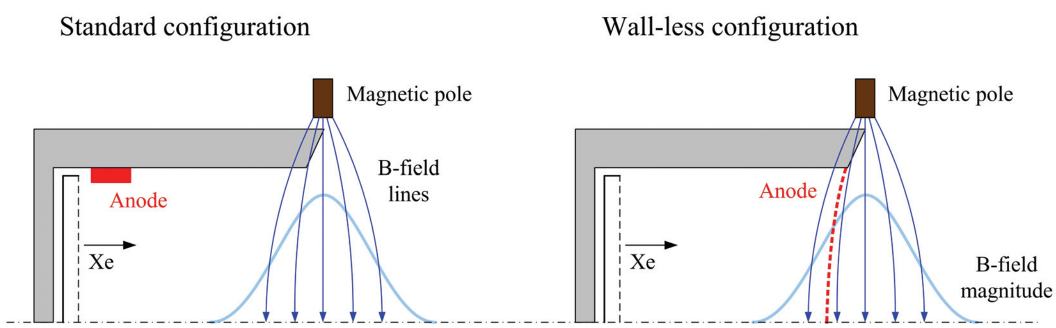

Figure 1. Schematic of a ISCT200 thruster in the standard (left) and wall-less (right) configurations.

The Hall thruster simulated in this work is the ISCT200 thruster. ISCT is an acronym for ICARE Small Customizable Thruster. The ISCT200 is a versatile 200 W-class Hall thruster using permanent magnets for generating the magnetic field instead of helical magnetizing coils[9,10]. The ISCT200 thruster can be operated in the standard (ST) and the wall-less (WL) configurations. The wall-less configuration is a recent and original approach to decrease plasma-wall interactions, hence prolonging the thruster lifetime[11,12]. The principle is to entirely shift the ionization and acceleration regions outside the cavity. Such unconventional design is named a Wall-Less Hall Thruster, or WL-HT in short[11,12,14]. This configuration was in fact first explored during the 90s in Ukraine by Kapulkin et al.[15,16] To shift both the ionization and the acceleration regions outside the thruster cavity, the anode is moved towards the channel exit. Schematics of the ISCT200 thruster both in the standard and the wall-less configurations are presented in Fig. 1. In the wall-less configuration the anode is a 1mm tick grid with 3mm in diameter circular holes placed exactly at the channel exit. The anode transparency is 0.68, which allows a homogeneous propellant gas distribution outside the channel. A photograph of the ISCT200 Hall thruster in WL configuration with its gridded anode at the channel exit is displayed in Fig. 2. The same figure shows the ISCT200-WL thruster firing with Xe at 1 mg/s and 200V discharge voltage in the NExET vacuum chamber. As can be seen, the plasma discharge is detached from the anode - the signature for an efficient confinement.

A wall-less ion source provides an ideal platform for the study of cross-field discharge configurations with the probes and optical diagnostic tools. The access it provides to key regions of the plasma facilitates a thorough investigation of plasma instabilities and small scale turbulence for a better understanding of the discharge physics and anomalous electron transport. Additionally, it allows studying these phenomena without the influence of wall processes such as secondary electron emission and sputtering. A WL Hall thruster is also an adequate configuration to make comparisons between experiments and computer simulations. Due to a simplified architecture, boundary conditions are easier to model, which permits to obtain more accurate and more reliable numerical outcomes. For all aforementioned reasons, the wall-less configuration has been selected to investigate the physics of rotating plasma instabilities in this work.

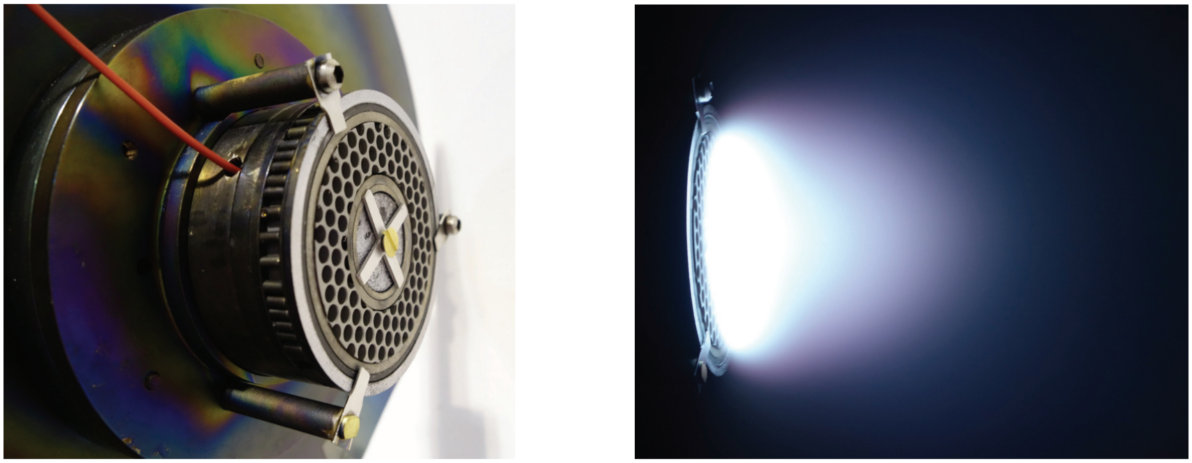

Figure 2. Picture of the ISCT200 Hall thruster in WL configuration with a gridded anode at the channel exit plane (left) and photograph of the thruster firing with Xe in the NExET test-bench.

III. The model

In this work, the self-consistent 3D-3V Particle-in-Cell simulation code STOIC (electrostatic Optimized particle In Cell)[4,8] has been applied to simulate the rotating spoke instability in the ISCT200 thruster operating in the wall-less configuration[13]. The simulation includes electrons, Xe^+ ions and neutral Xenon atoms. All relevant collisional processes are included in the model: Coulomb collisions between charged particles; electron-neutral elastic, ionization and excitation collisions; ion-neutral momentum transfer and charge exchange collisions and neutral-neutral elastic collisions. The dynamics of the background neutral gas is selfconsistently resolved with direct simulation Monte Carlo (DSMC). The model is full-3D - 3 spatial and 3 velocity components are resolved. It utilizes an equidistant Cartesian grid which explicitly assures momentum conservation and zero self forces.

The computational domain represents a cuboid with length $Z_{\max} = 50\,\text{mm}$ and sides $X_{\max} = Y_{\max} = 70\ \text{mm}$. Z axis is directed along the thruster symmetry axis. The sketch of the computational domain together with magnetic field topology and particle sources is shown in Fig. 3. The plane $Z = 0$ correspond to the channel exit, where the anode (red) is placed. The ring anode is mapped with the Cartesian mesh. All boundaries of the computational domain are assumed to be metallic. All metal elements in the simulation, except for the anode are at ground potential (blue). At the anode, a voltage of $U_a = 90 - 250$ V is applied. The neutrals are injected into the system through the anode with the mass flow rate $\dot{m} = 0.8 - 1.3$ mg/s and $T_n = 400$ K. Electrons with a Maxwellian distribution and a temperature $T_e = 2$ eV are introduced into the system in the source region $42\,\text{mm} < Z < 46\,\text{mm}$, $26\,\text{mm} < R < 30\,\text{mm}$ with uniform density and the constant current $I_c = 0.25$ A, simulating the thruster cathode. All surfaces in the simulation are assumed to be absorbing for electrons and ions. No secondary electron emission is assumed in the simulation. The neutrals are lost on all surfaces, except for the anode plane, where they are re-launched with Maxwellian distribution with the temperature $T_n = 400$ K.

To reduce the computational time the size of the system is scaled down by a factor of 10. In order to preserve the ratio of the particles mean free paths and the gyroradii to the system length, the collisions cross-sections and the magnetic field are increased by the same factor 10.

An equidistant computational grid 70x70x50 was used in the simulation. The total number of computational particles in the simulation was about 20000000. The cell size $\Delta x = \Delta y = \Delta z = 10^{-1}$ mm in the simulation was chosen to ensure that it is smaller than the smallest Debye length in the system. The time step was set to $\Delta t = 5.6 \cdot 10^{-12}$ s in order to resolve the electron plasma frequency. The simulation was carried on a 16-processor Intel Xeon workstation. The duration of the typical run was about 15 days. About 10^7 time steps were performed which corresponds to a simulated time of 56 µs.

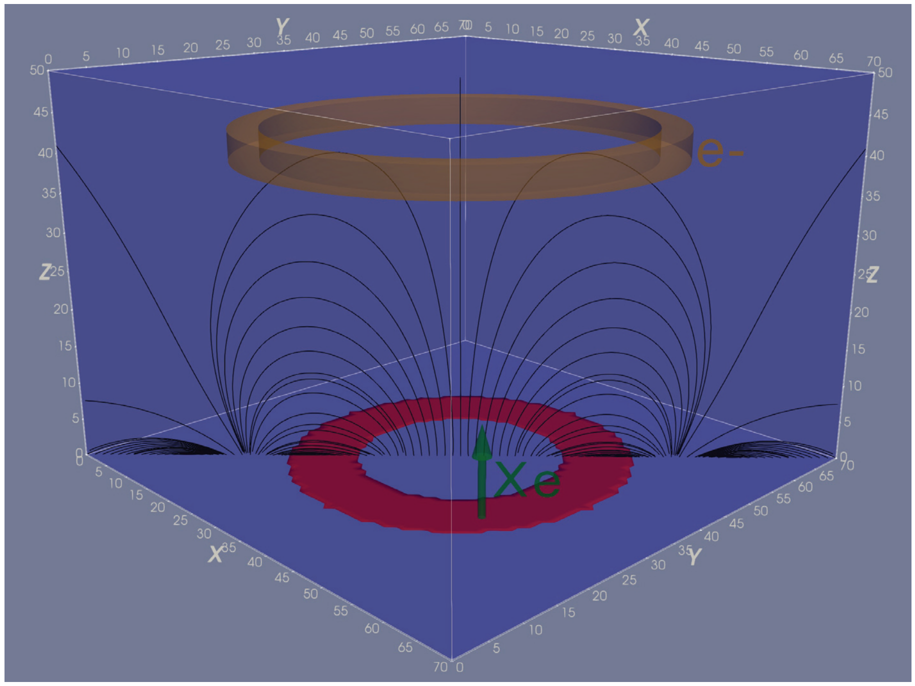

Figure 3. Computational domain with magnetic field topology and particle sources.

IV. Simulation results

During the simulations low-frequency rotating plasma instabilities (spokes) were observed in the ionization region close to the anode. For most of the simulated regimes the m = 1 mode was present with a few occurrencies of m = 2 mode. The spokes were rotating both in the *E*x*B* (clockwise) and in counter-*E*x*B* directions. The spoke rotation velocity was in the range of 3.8-6.3 km/s, which corresponds to the rotation frequency of 34-56 Hz for unscaled geometry. This is about a factor of 3 faster than observed in the experiment[13]. Such discrepancy with the experimental results may be caused by the proximity of the boundaries to the plasma in the simulations or by the geometrical scaling. The examples of the m=1 and m=2 spokes can be seen in Figures 4-6 in the electron density XY cross-sections 2.5 mm up from the anode.

In Figures 7-10 the dynamics of the electron and neural density, plasma potential and ionization rate 4 mm up from the anode and the electron current density at the anode for the spoke rotating in the *E*x*B* direction are presented. The spoke rotation is associated with strong azimuthal depletion of the neutral gas, which indicates the ionization nature of the spoke instability. In the potential dynamics, besides the macroscopic low frequency (LF) spoke fluctuations at the spoke boundaries with corresponding azimuthal electric field about 20 V/cm, one can see the short scale ~2 mm high frequency (HF) oscillations with the electric field up to 200 V/cm (both axial and azimuthal) in the spoke bulk. The mean electric field in the spoke bulk is about 10 V/cm (both axial and azimuthal), thus these HF oscillations should disrupt the regular azimuthal electron *E*x*B* drift inside the spoke. Such short-scale oscillations manifest themselves in the electron temperature profile inside the spoke as well, so they obviously contribute to the electron transport through the spoke. The macroscopic azimuthal electric field at the spoke front is directed clock-wise, so the corresponding electron *E*x*B* drift is directed towards the anode contributing to the anode current. At the back of the spoke the macroscopic *E*-field is directed opposite and thus causes the *E*x*B* drift in *Z* direction, up from the anode, decreasing the anode current. Comparing the electron current density profile at the anode with the electron density above the anode one can see that indeed electron transport at the spoke front is more efficient.

In Fig. 11 the frequency spectrum of the plasma density is presented. In addition to the spoke frequency, 520 kHz (due to geometric scaling rotation frequency is increased by factor of 10 compared with the real system) and its harmonics, the high frequency oscillations in 1-10 MHz range can be seen. These high frequency oscillations are likely to be responsible for the electron cross-field transport inside the spoke.

In Fig. 12 the evolution of distribution function of ion aizmuthal velocity inside the spoke (4 mm up from the anode) during two spoke rotation cycles is plotted together with the evolution of electric potential and the ion density. As one can see in Fig. 12, the ion azimuthal velocity distribution function (VDF) is strongly affected by both the LF and HF oscillations. As expected the macroscopic azimuthal electric fields at spoke front and back (LF oscillations) accelerate the ions in the opposite directions. The HF potential oscillations in the spoke bulk lead to high frequency modulation of the ion VDF. As the spoke potential growth takes much longer than potential fall, the mean ion azimuthal velocity is positive (in the *E*x*B* direction) for large part of the cycle. The averaged over the cycle ion azimuthal velocity is around 103 m/s, which is much slower than spoke rotation velocity 6.3 km/s. These observations agree with time resolved LIF measurements of ion VDF in ISCT200-WL thruster[13].

In Figure 13 the isosurfaces of the electron density and the electric potential directly over the anode are presented. Here it is clearly visible how asymmetry in the electron density due to the spoke is leading to the asymmetry in plasma potential. As the electric field is normal to the potential isosurfaces and the magnetic field lines are essentially lying on the isosurfaces, the electron *E*x*B* drift orbits should stick to surfaces of the constant potential. Thus asymmetry in potential distribution should lead to asymmetry in the electron drift motion in the spoke region. The isosurface of the $\varphi = 250\,\text{V}$ in the spoke bulk is strongly distorted due HF oscillations, thus, again, one should not expect the regular azimuthal electron *E*x*B* drift in this region.

In Figures 14-20 the trajectories of the test electrons in the spoke region during the 84 ns are plotted. For orientation purpose the potential isosurface of $\varphi = 200$ V is plotted as well. As one can see in Figures 14-16 in the spoke bulk electron motion has clear diffusive pattern, when both the particle position and the energy are changing randomly. (The electron energy can by estimated by its gyroradius). The test electrons are not collided with other particles, their motion is completely defined by background electric and magnetic fields. Thus, indeed, strong HF plasma oscillations in the spoke bulk disrupt the regular *E*x*B* drift of the electrons, and lead to diffusion-like electron motion in this region. As a result of this diffusive motion some electrons are reaching the anode (Fig. 16), contributing to the discharge current. Thus one can claim that in the simulation the electron current through the bulk of the spoke is clearly diffusive. Analyzing the electron motion at the spoke front (Figures 17-18) one can distinguish clear *E*x*B* drift pattern in the spoke macroscopic electric field overlaid with the oscillation between magnetic mirrors along the magnetic field lines. The *E*x*B* drift in the Z-direction due to spoke azimuthal field as it was expected directed toward the anode. In Figures 17-18 one can see how as a result of this drift motion the electrons are reaching the anode. Thus one can claim that the electron current through the spoke front is due to *E*x*B* drift in the sheath macroscopic field. In Figures 19-20 one can see the motion of the electrons at the sheath back. It is clearly an *E*x*B* drift combined with the bouncing between magnetic mirrors along the B-field lines. As it was expected, at spoke back the electron *E*x*B* drift directed along Z direction, up from the anode. The electron drift orbits in Figures 19-20 are located along the equipotential surfaces, repeating their asymmetry, caused by the spoke.

V. Conclusion

3D PIC MCC simulations were used to study the rotating spoke in the ISCT200-WL thruster. The spokes rotating with the velocity 3.8 - 6.3 km/s were observed, which is factor ~3 faster than in the experiment. For most of the simulated regimes the m = 1 mode was present with a few occupancies of m = 2 mode. In the simulation the spokes were rotating both in the *E*x*B* and in counter- *E*x*B* directions.

The spoke rotation is associated with azimuthal depletion of the neutral gas, which indicates ionization nature of the spoke instability. Strong high-frequency electric field oscillations (1-10 MHz), the length scale ~2mm and the amplitudes up to 200 V/cm were observed inside the spoke.

In the simulations the electron cross-field transport in the spoke bulk was caused by diffusion in high-frequency, short scale electric field. Whereas the electron conductivity at the spoke front was due to *E*x*B* drift toward the anode in the low-frequency macroscopic spoke electric field

Further joint efforts of simulation and experiment are necessary for clarification of the phenomena underlying the spoke formation and the dynamics.

Acknowledgments

This work was supported by European Office of Aerospace Research and Development (EOARD) grant FA9550-15-1-0281.

References

[1]J. P. Boeuf. Rotating structures in low temperature magnetized plasmas - insight from particle simulations, *Frontiers in Physics*, Vol 2, Art. 74, 2014, pp. 1-17.

[2]G. S. Janes and R. S. Lowder, "Anomalous electron diffusion and ion acceleration in a low-density plasma," *Phys. Fluids*, Vol. 9, No.6, 1966, pp. 1115–1123.

[3]Y. V. Esipchuk, A. I. Morozov, G. N. Tilinin, and A. V.Trofimov, "Plasma oscillations in closed-drift accelerators with an extended acceleration zone," *Sov. Phys.-Tech. Phys.*, vol. 43, 1973, pp. 1466–1473.

[4]K. Matyash , R. Schneider , O. Kalentev , Y. Raitses and N. J. Fisch, "Numerical investigations of a cylindrical Hall thruster," *32nd International Electric Propulsion Conference*, 2011, IEPC-2011-070.

[5]M. S. McDonald and A. D. Gallimore, "Parametric investigation of the rotating spoke instability in Hall thrusters," *32nd International Electric Propulsion Conference*, 2011, IEPC-2011-242.

[6]J. B. Parker, Y. Raitses, and N. J. Fisch, "Transition in electron transport in a cylindrical Hall thruster," *Appl. Phys. Lett.*, vol. 97, No. 9, 2010, p. 091501.

[7]C. L. Ellison, Y. Raitses and N. J. Fisch, "Cross-field electron transport induced by a rotating spoke in a cylindrical Hall thruster," *Phys. Plasmas*, 19, 2012, 013503.

[8]K. Matyash, R. Schneider, S. Mazouffre, Y. Raitses, and A. Diallo, "3D simulation of rotating spoke in a Hall thruster," *33rd International Electric Propulsion Conference*, 2013, IEPC-2013-307.

[9]S. Mazouffre, G. Bourgeois, K. Dannenmayer, and A. Lejeune, "Ionization and acceleration processes in a small, variable channel width, permanent-magnet Hall thruster," *J. Phys. D: Appl. Phys*., vol. 45, No. 18, 2012, p.185203.

[10]A. Lejeune, G. Bourgeois, and S. Mazouffre, "Kr II and Xe II axial velocity distribution functions in a cross-field ion source," *Phys. Plasmas*, Vol. 19, No. 7, 2012, p. 073501.

[11]S. Mazouffre, S. Tsikata, and J. Vaudolon, "Development and experimental characterization of a wall-less Hall thruster," *J. Appl. Phys.*, Vol. 116, No.24, 2014, p. 243302.

[12]J. Vaudolon, S. Mazouffre, C. Henaux, D. Harribey, and A. Rossi. "Optimization of a wall-less Hall thruster," Appl. Phys. Letter, Vol. 107, No. 17, 2015, p. 174103.

[13]S. Mazouffre, L. Grimaud, S. Tsikata, K. Matyash and R. Schneider, "Investigation of rotating spoke instabilities in a wall-less Hall thruster. Part I: Experiment," *35th International Electric Propulsion Conference*, 2017, IEPC-2017-248.

[14]B. Karadag, S. Cho, Y. Oshio, Y. Hamada, I. Funaki, and K. Komurasaki, "Preliminary Investigation of an External Discharge Plasma Thruster," *In Proceedings of the 52nd Joint Propulsion Conference*, AIAA paper 2016-4951, Salt Lake City, Utah, 2016.

[15]A. M. Kapulkin, A. D. Grishkevich, and V. F. Prisnyakov, "Outside electric field thruster," *Proceedings of the 45th IAF Congress; Space Technol*., Vol. 15. (Pergamon, UK), 1995, pp. 391-394.

[16]V. F. Prisnyakov, A. N. Petrenko, A. M. Kapulkin, I. N. Statsenko, A. I. Kondratiev, and S. N. Kulagin, "The review of the works on electrical propulsion thrusters development and investigation carried out at the Dnepropetrovsk State University,". *24th International Electric Propulsion Conference*, 1995, IEPC-1995-12.

[17]A. Gupta, "WSMP: Watson Sparse Matrix Package. Part I – direct solution of symmetric sparse systems", IBM RC21886 (98462) 2000.

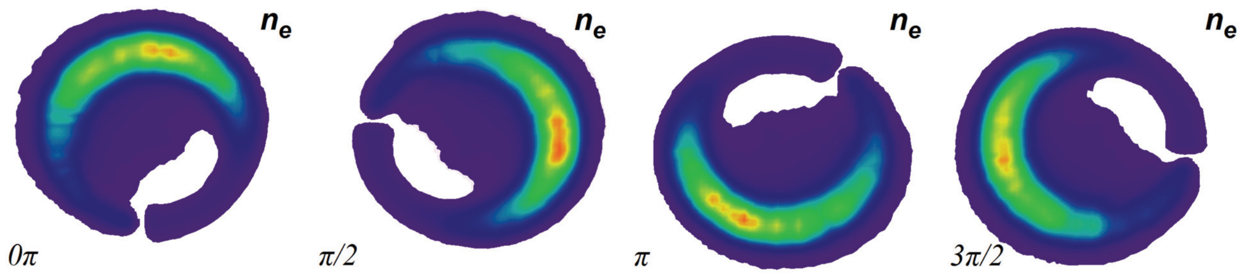

Figure 4. Evolution of the plasma density 2.5 mm up from the anode during the spoke cycle. U_a = 250 V, $\dot{m}$ = 1 mg/s. The spoke m = 1 rotates in the ExB direction with velocity 6.3 km/s.

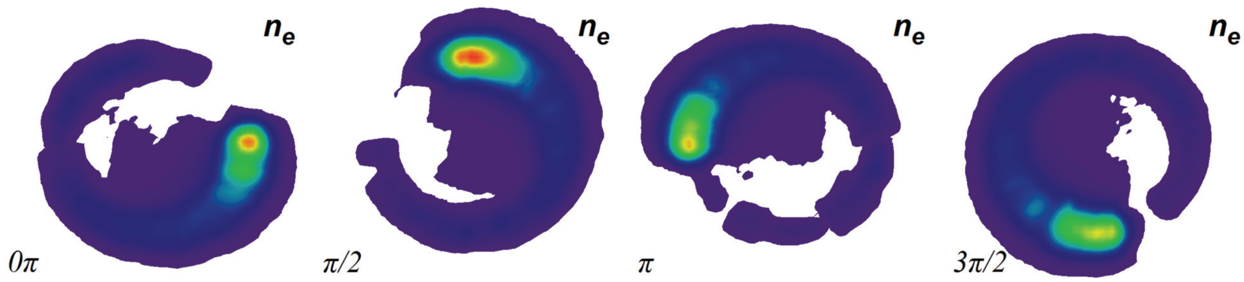

Figure 5. Evolution of the plasma density 2.5 mm up from the anode during the spoke cycle. U_a = 175 V, $\dot{m}$ = 1 mg/s. The spoke m = 1 rotates opposite to ExB direction with velocity 3.8 km/s.

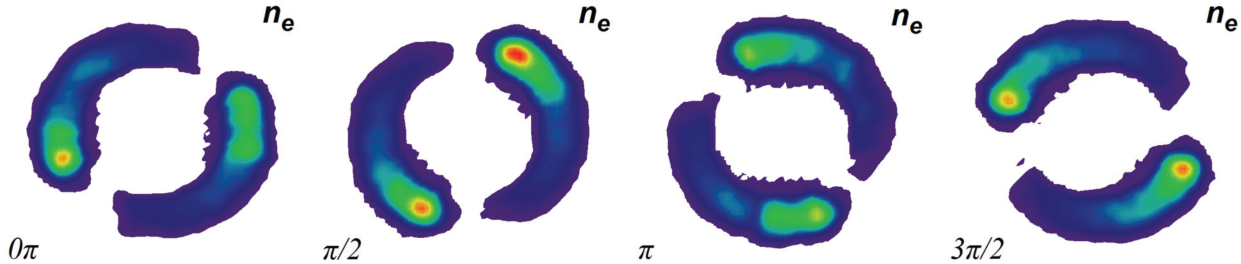

Figure 6. Evolution of the plasma density 2.5 mm up from the anode during the spoke cycle. U_a = 120 V, $\dot{m}$ = 1.3 mg/s. The spoke m = 2 rotates opposite to ExB direction with velocity 4.5 km/s.

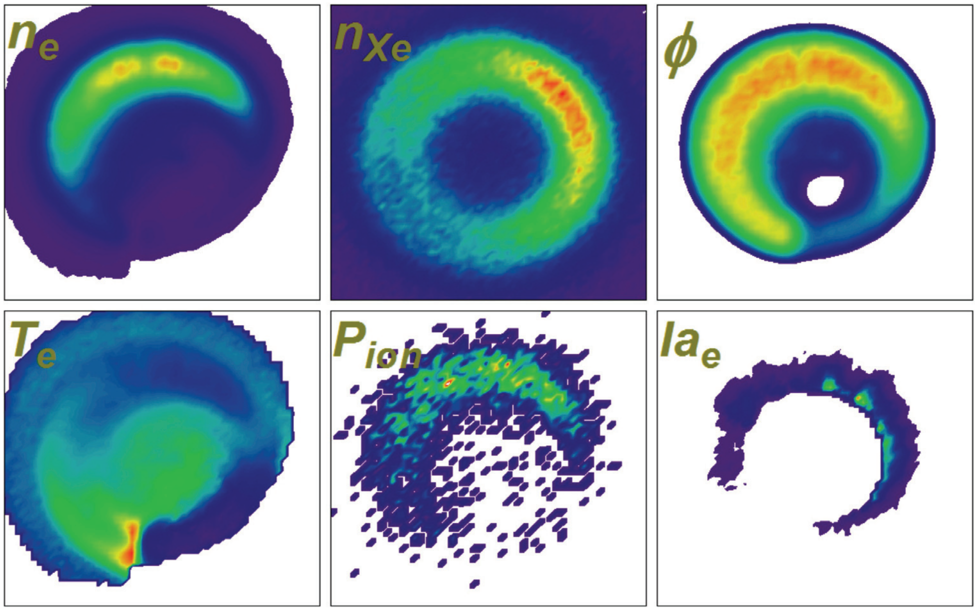

Figure 7. Electron and neural density, plasma potential (above), electron temperature, ionization rate 4 mm up the anode and the electron current density at the anode (below) at $\varphi = 0$ of the spoke rotation cycle. U_a = 250 V, $\dot{m} = 1$ mg/s.

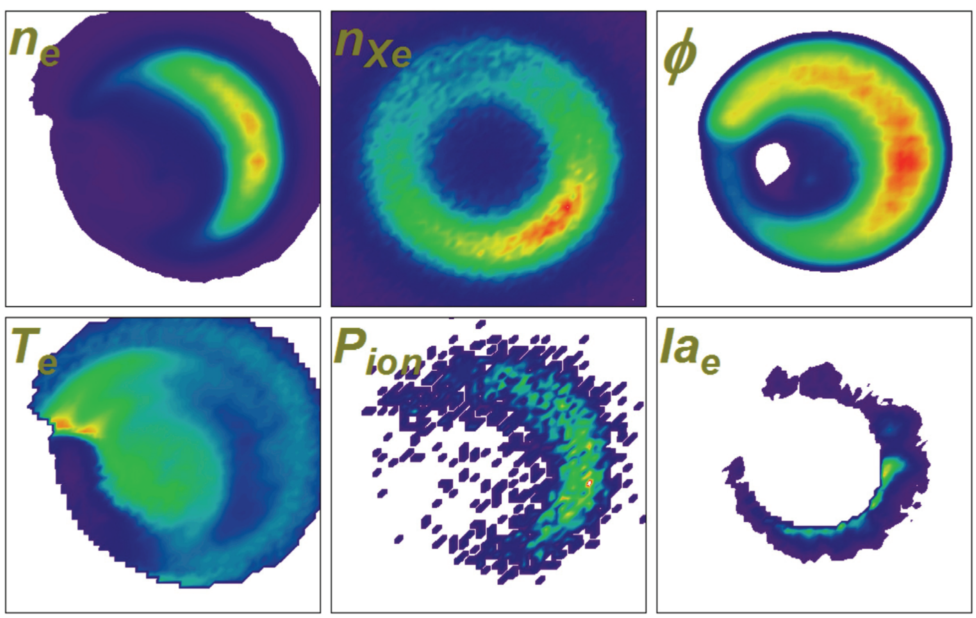

Figure 8. Electron and neural density, plasma potential (above), electron temperature, ionization rate 4 mm up the anode and the electron current density at the anode (below) at $\varphi = \pi/2$ of the spoke rotation cycle. U_a = 250 V, $\dot{m} = 1$ mg/s.

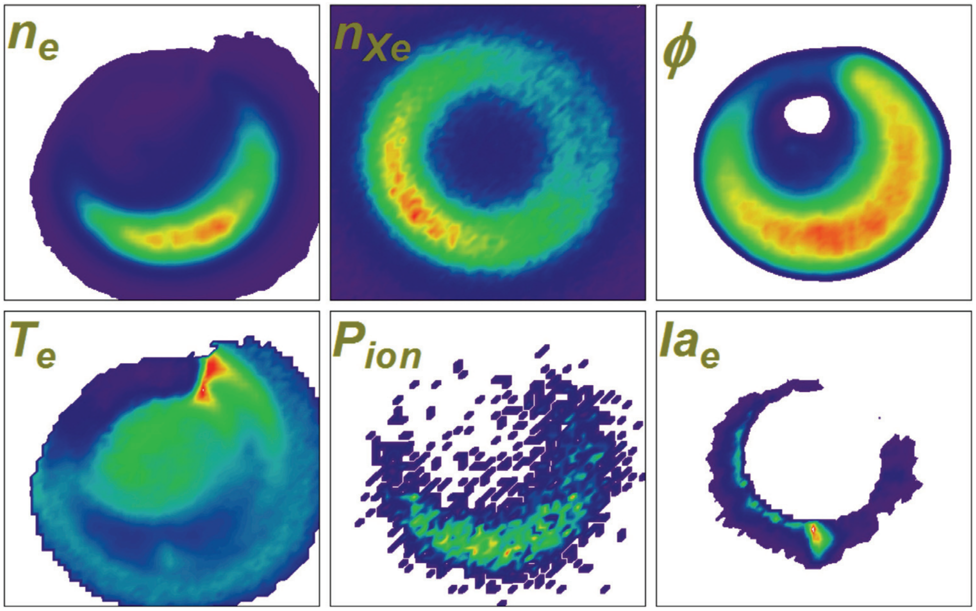

Figure 9. Electron and neural density, plasma potential (above), electron temperature, ionization rate 4 mm up the anode and the electron current density at the anode (below) at $\varphi = \pi$ of the spoke rotation cycle. U_a = 250 V, $\dot{m} = 1$ mg/s.

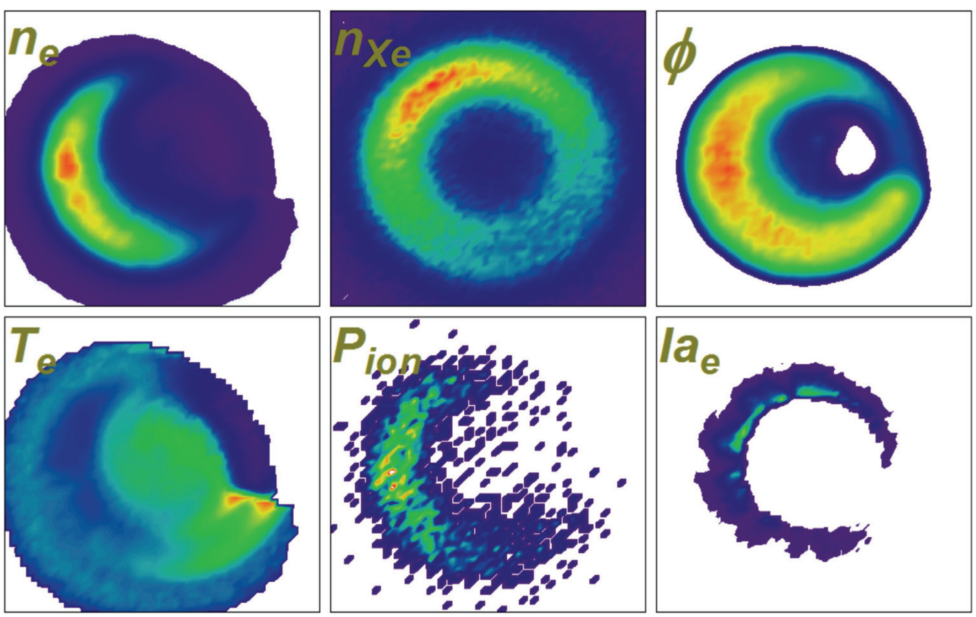

Figure 10. Electron and neural density, plasma potential (above), electron temperature, ionization rate 4 mm up the anode and the electron current density at the anode (below) at $\varphi = 3\pi/2$ of the spoke rotation cycle. U_a = 250 V, $\dot{m} = 1$ mg/s.

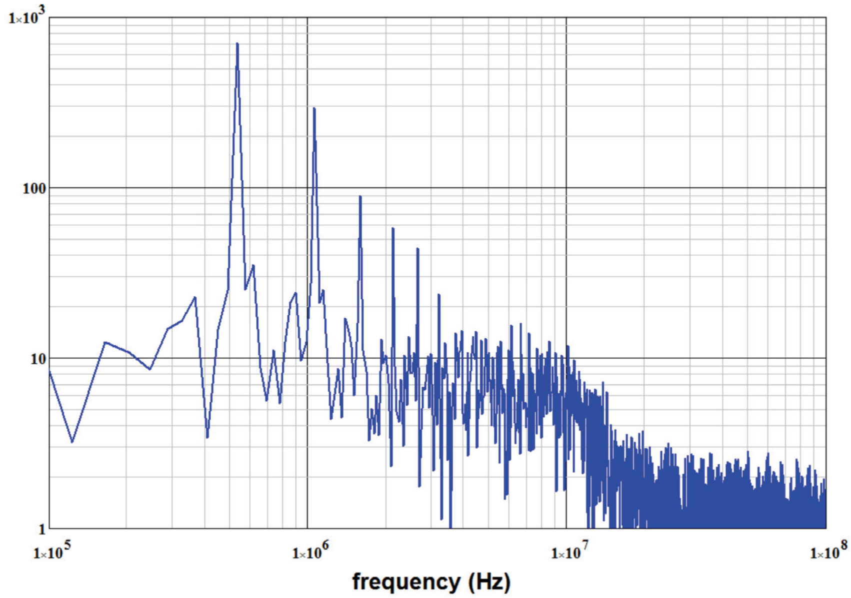

Figure 11. The frequency spectrum of the plasma density oscillations taken inside the spoke 4 mm up from the anode.

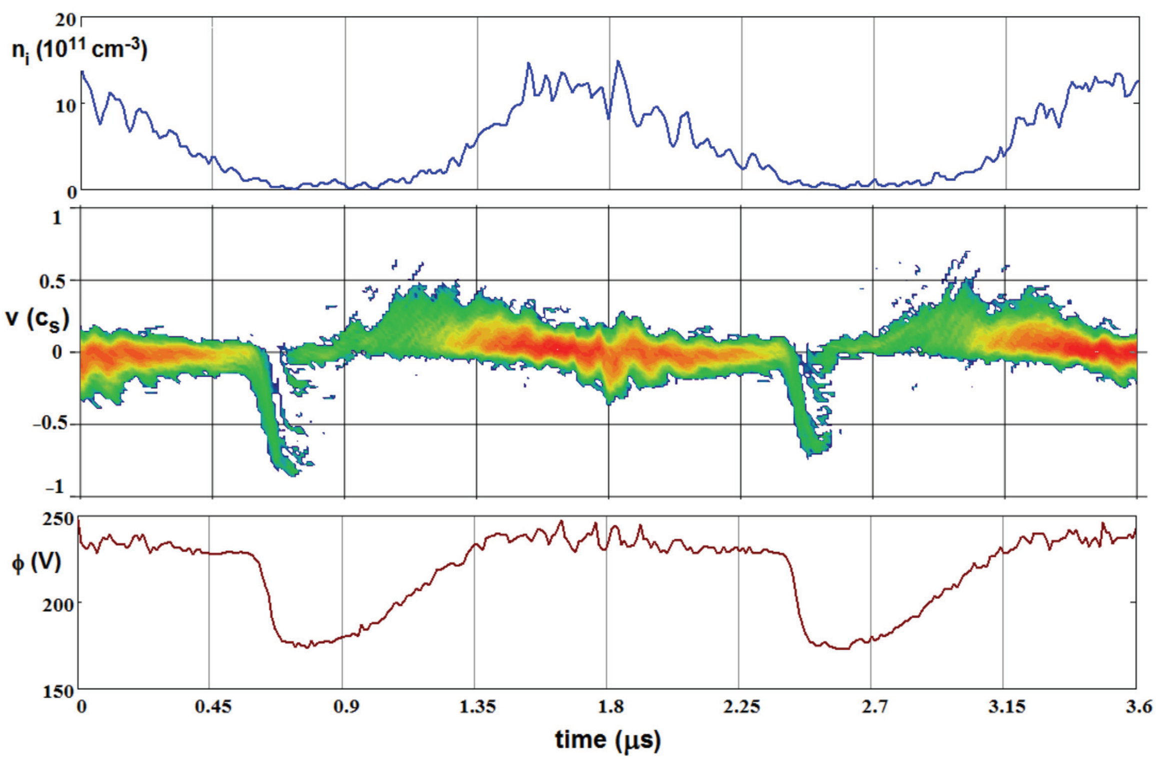

Figure 12. Time-dependent ion VDF during two rotation cycles of the plasma instability (middle) 4 mm up the anode. The ion acoustic speed c_s is equal to 5422 m/s here. Also shown: the time evolution of the ion density (upper plot) and the time evolution of the electrical potential (lower plot). U_a = 250 V, $\dot{m}$ = 1 mg/s.

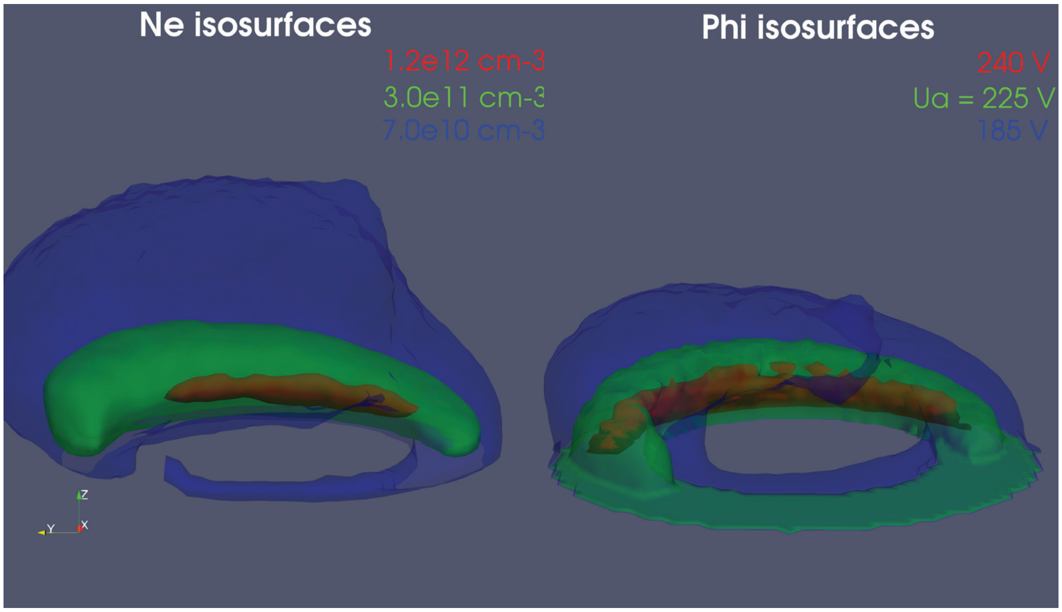

Figure 13. The isosurfaces of the electron density and the plasma potential over the anode. The spoke m = 1 rotates in the ExB direction (clockwise). U_a = 250 V, $\dot{m}$ = 1 mg/s.

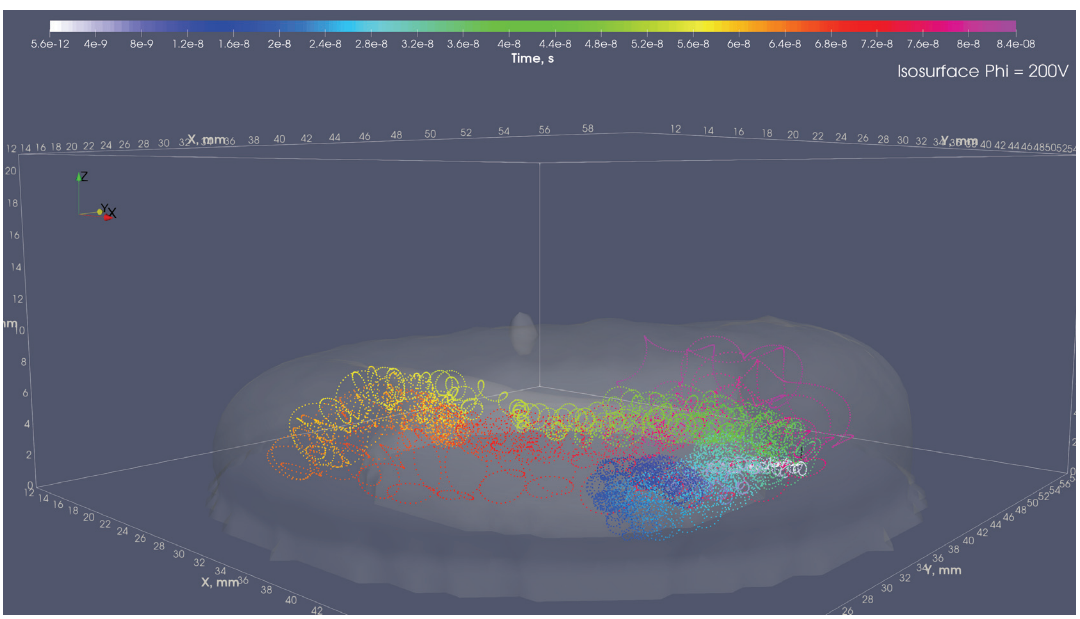

Figure 14. Trajectory of the test electron in the spoke bulk during 84 ns. For orientation purpose the potential isosurface φ = 200 V is plotted as well. The spoke m = 1 rotates in the ExB direction (clockwise). U_a = 250 V, $\dot{m}$ = 1 mg/s.

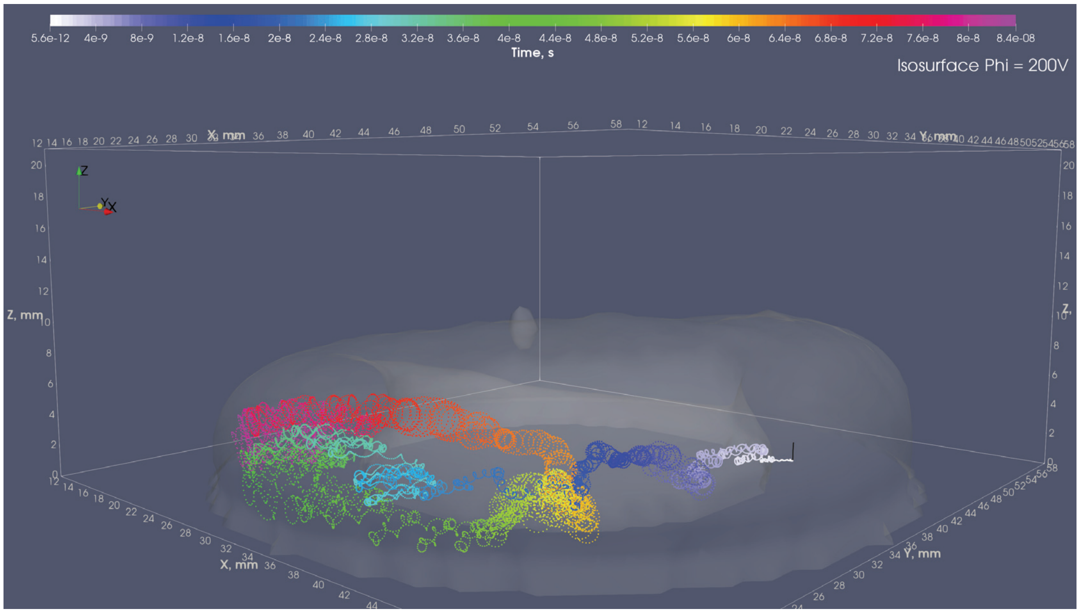

Figure 15. Trajectory of the test electron in the spoke bulk during 84 ns. For orientation purpose the potential isosurface $\varphi = 200$ V is plotted as well. The spoke m = 1 rotates in the ExB direction (clockwise). U_a = 250 V, $\dot{m} = 1$ mg/s.

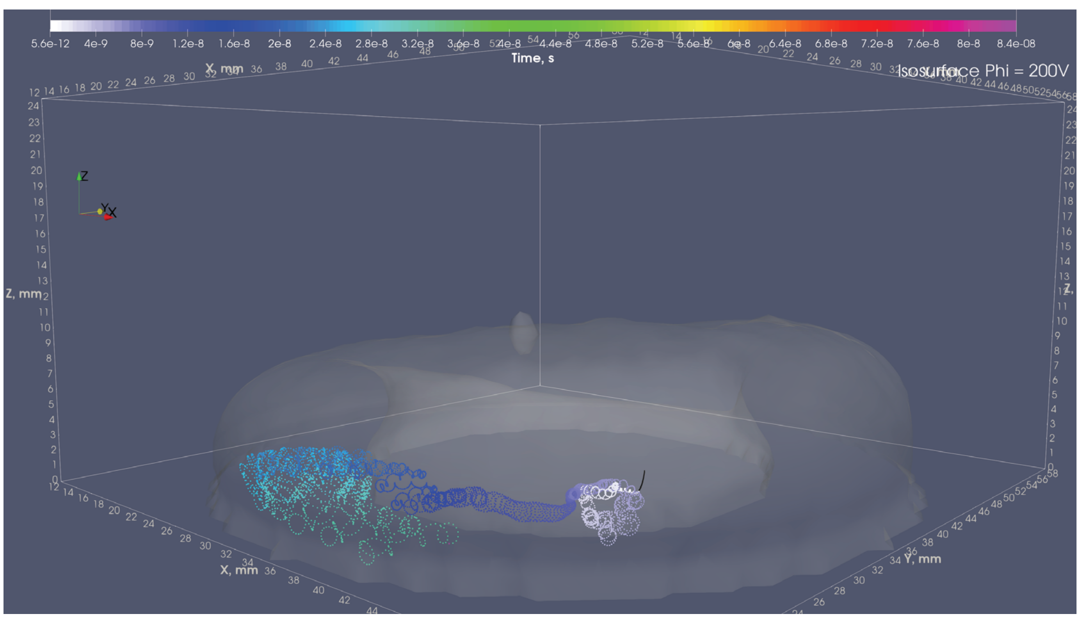

Figure 16. Trajectory of the test electron in the spoke bulk during 84 ns. For orientation purpose the potential isosurface $\varphi = 200$ V is plotted as well. The spoke m = 1 rotates in the ExB direction (clockwise). U_a = 250 V, $\dot{m} = 1$ mg/s.

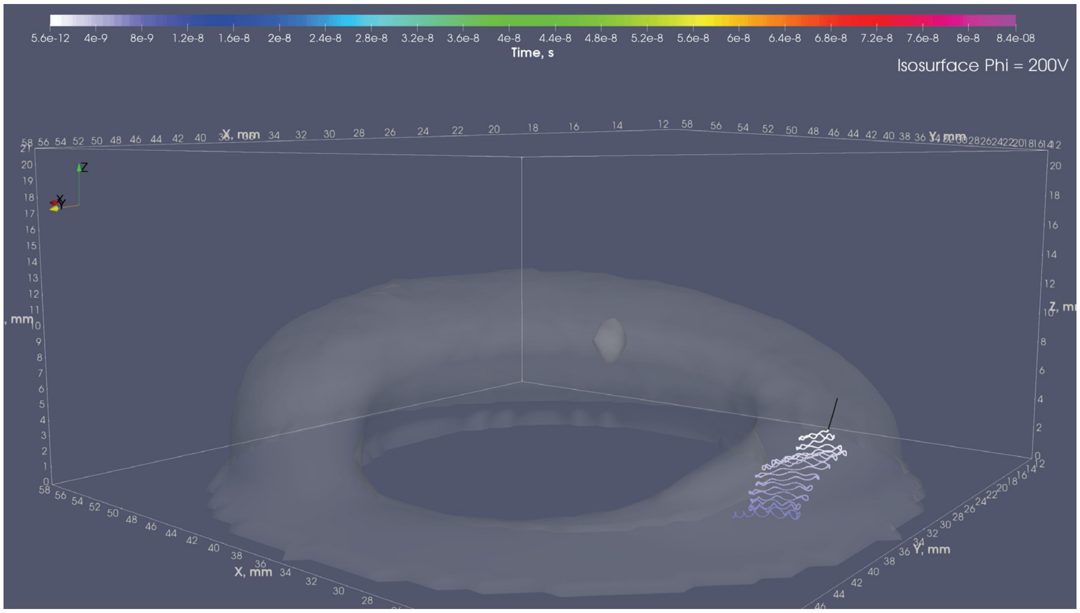

Figure 17. Trajectory of the test electron at the spoke front during 84 ns. For orientation purpose the potential isosurface $\varphi = 200$ V is plotted as well. The spoke $m = 1$ rotates in the *E*x*B* direction (clockwise). U_a = 250 V, $\dot{m} = 1$ mg/s.

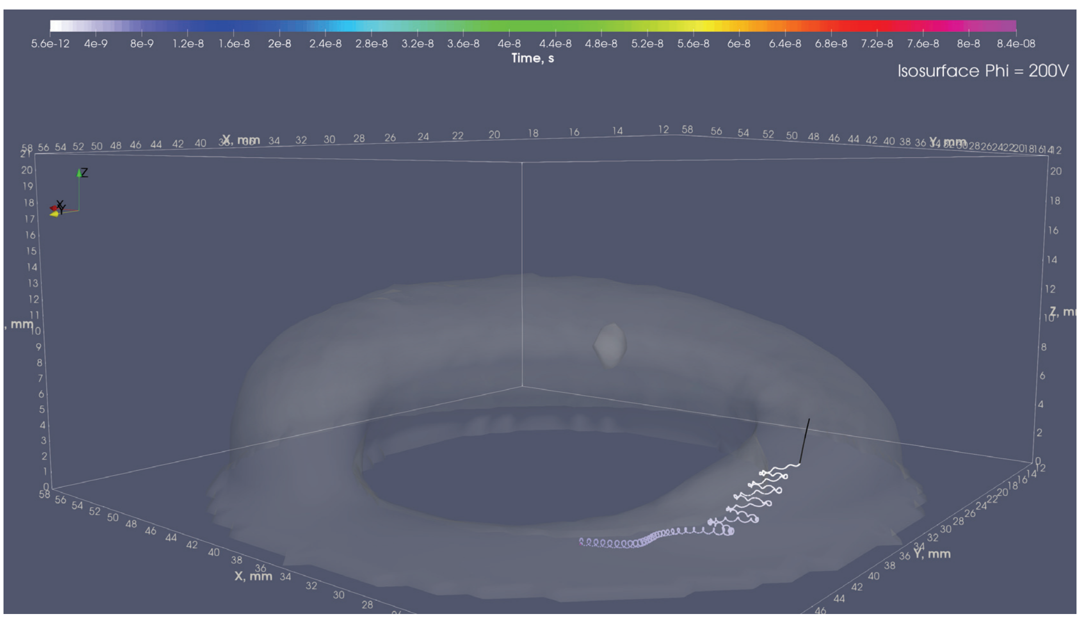

Figure 18. Trajectory of the test electron at the spoke front during 84 ns. For orientation purpose the potential isosurface $\varphi = 200$ V is plotted as well. The spoke $m = 1$ rotates in the *E*x*B* direction (clockwise). U_a = 250 V, $\dot{m} = 1$ mg/s.

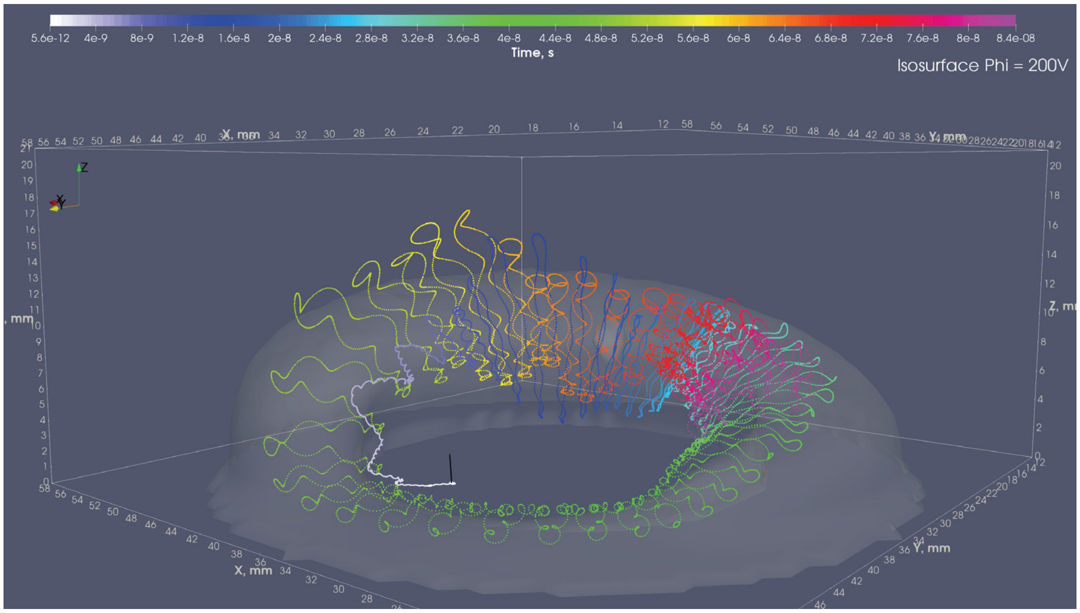

Figure 19. Trajectory of the test electron at the spoke back during 84 ns. For orientation purpose the potential isosurface $\varphi = 200$ V is plotted as well. The spoke $m = 1$ rotates in the ExB direction (clockwise). U_a = 250 V, $\dot{m} = 1$ mg/s.

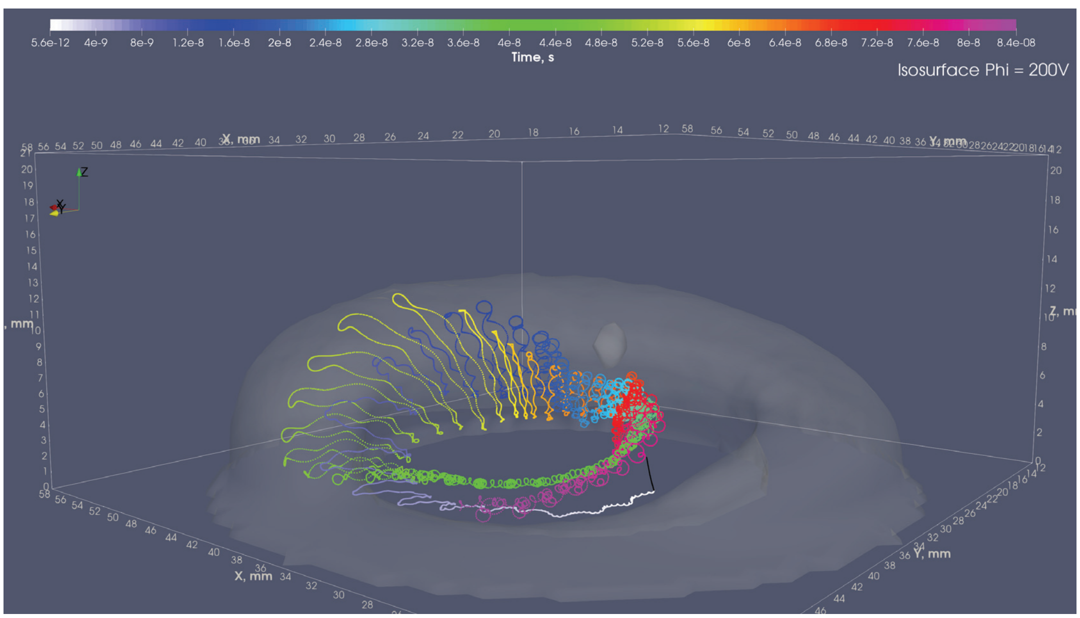

Figure 20. Trajectory of the test electron at the spoke back during 84 ns. For orientation purpose the potential isosurface $\varphi = 200$ V is plotted as well. The spoke $m = 1$ rotates in the ExB direction (clockwise). U_a = 250 V, $\dot{m} = 1$ mg/s.